Dark matter chaos in the Solar System

J.Lages
Institut UTINAM, Observatoire des Sciences de l'Univers THETA, CNRS & Université de Franche-Comté, 25030 Besançon, France

D.L.Shepelyansky
Laboratoire de Physique Théorique du CNRS, IRSAMC, Université de Toulouse, UPS, F-31062 Toulouse, France

(Dated: November 5, 2012)

We study the capture of galactic dark matter particles in the Solar System produced by rotation of Jupiter. It is shown that the capture cross section is much larger than the area of Jupiter orbit being inversely diverging at small particle energy. We show that the dynamics of captured particles is chaotic and is well described by a simple symplectic dark map. This dark map description allows to simulate the scattering and dynamics of 10^{14} dark matter particles during the life time of the Solar System and to determine dark matter density profile as a function of distance from the Sun. The mass of captured dark matter in the radius of Neptune orbit is estimated to be $2 \cdot 10^{15} g$. The radial density of captured dark matter is found to be approximately constant behind Jupiter orbit being similar to the density profile found in galaxies.

PACS numbers: 95.35.+d, 05.45.Ac, 96.25.De, 96.30.Vb

A galactic wind of dark matter particles (DMP) [1] flies through the Solar System and a part of it becomes captured due rotation of planets around the Sun. The capture process, dominated by Jupiter, is related to the nontrivial aspects of the restricted three-body problem [2]. We demonstrate that this process is described by a simple dynamical symplectic map [3, 4] which allows to perform extensive numerical simulations of DMP capture. Our studies show that the capture cross section is much larger than the area of Jupiter orbit being diverging as an inverse square of DPM velocity in agreement with recent analytical estimates [5]. The dynamical map analysis allows to simulate DMP capture and ejection on the whole life time scale of the Solar System for 10^{14} DMP being more efficient than the direct simulations of DPM dynamics [6]. Our approach provides a DMP density distribution in the Solar System with other features of dynamics at present time after 4.5 billion years evolution of the Solar System. This DMP distribution is similar to those found in galaxies [7]. The dynamics of DMP is shown to be chaotic having certain similarities with a chaotic comet motion in the Solar System discussed in [8–12].

Following [1] we assume that in a vicinity of the Solar System (SS) the velocity distribution of DMP has a Maxwell form $f(v)dv = \sqrt{54/\pi} v^2/u^3 \exp(-3v^2/2u^2)dv$ with the average module velocity $u \approx 220 km/s$. During a scattering of DMP on the Sun its rescaled total energy $w = -2E/m_d v_p^2$ is changed due to planetary rotation. The main contribution is given by Jupiter [9] and hence we base our studies on the case of one planet measuring DMP parameters in units of planet radius r_p and velocity v_p taken as unity, DMP mass $m_d = 1$. The studies of comet dynamics [8–10] in SS with one rotating planet show that it is well described by a symplectic map and thus a DMP dynamics over an extended orbit is also described by that type of map. This dark map has a form similar to the Halley map [9]:

$$w_{n+1} = w_n + F(x_n) \ , \ \ x_{n+1} = x_n + w_{n+1}^{-3/2} \ , \qquad (1)$$

where $x_n = t_n/T_p \ (mod 1)$ is given by time t_n taken at the moment of DMP $n-th$ passage through perihelion, T_p is the planet period. The second equation in (1) follows from the Kepler law for the DMP orbital period. The amplitude of kick function $F(x)$ is proportional to the ratio of planet mass m_p to the Sun mass M_S ($F \sim m_p/M_s$) [8, 9]. Its shape depends on DMP perihelion distance q, inclination angle θ between the planetary plane (x, y) and DMP plane, and perihelion orientation angle φ. However, $F(x)$ is independent of energy w for $1/|w| \gg r_p = 1$. Thus the dark map describes DMP dynamics for bounded and unbounded energies as well as its capture process corresponding to a transition from positive $w < 0$ to negative energies $w > 0$.

Our direct numerical simulations of Newton equations confirms this map description by F-function as it is shown in Fig. 1 for various values of q, θ, φ, including the Halley comet case analyzed in [9]. In agreement with the theory [8] the maximum F_{max} drops exponentially for $q \gg r_p$ so that only DMP with $q < 2r_p$ can be effectively captured. At $q \gg r_p$ we find $F \sim \sin 2\pi x$ in agreement with [8]. The visible peaks in F_{max} correspond to close encounters between DPM and planet happening at rather specific angles for $q \leq r_p$. We will see later that such events give a small contribution in the capture cross section σ. In fact, $F-$function contribution comes from encounter distances of the order of r_p thus being much larger than the radius of the planet body r_b. This analytical result [5, 8, 9, 13] is in agreement with the detailed numerical simulations [6] invalidating previous numerical studies [14, 15] which considered contributions only from r_b scale. Finally, we note that the dark map gives an effi-

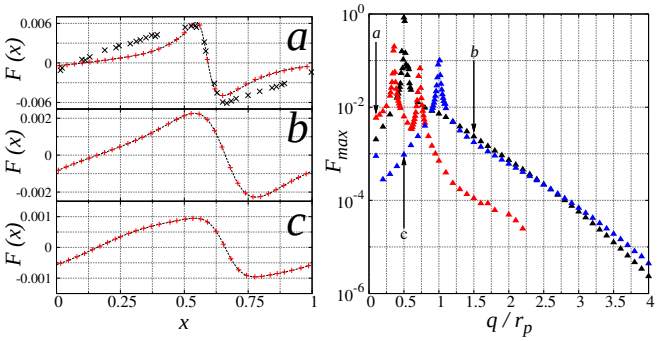

FIG. 1: *Left panel*: dependence of kick function $F(x)$ on Jupiter phase x for DMP orbit parameters shown by pluses: *a*) $q = 0.11$, $\theta = 2.83$, $\varphi = 1.95$ of the Halley comet case; here crosses show data for the Halley comet with all SS planets taken from Fig.1 of [9]; *b*) $q = 1.5$, $\theta = 0.7$, $\varphi = \pi/2$; *c*) $q = 0.5$, $\theta = \pi/2$, $\varphi = 0$; curves show fit functions of numerical data marked by pluses. *Right panel*: dependence of maximal amplitude F_{max} on q for a, b, c cases of left panel.

cient but approximate description. For the exact dynamics there is a slow variation of DMP orbital momentum ℓ and $q = \ell^2/(2r_p v_p^2)$ and angles θ, φ [11]. However, the rate of these variations is rather slow being proportional to m_p/M_S and does not affect significantly the chaotic diffusion in energy. Also numerical simulations of DMP dynamics point on a small global variation of q [6]. A similar situation appears in a microwave ionization of Rydberg atoms where it is known that the Kepler map in energy gives a good description of ionization process of 3D-atoms [13]. Also the DPM flow $f(v)dv$ performs an averaging over all ℓ, θ, φ values and hence a variation of these parameters is averaged out.

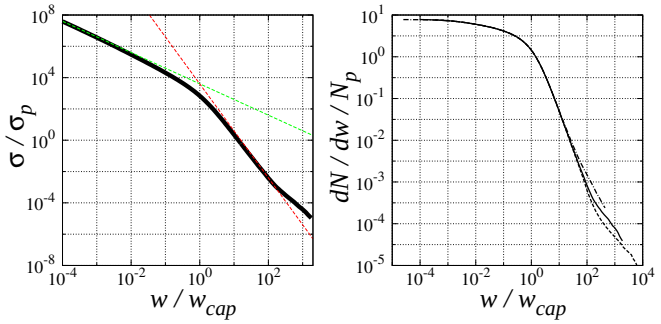

FIG. 2: *Left panel*: Dependence of capture cross section σ for Jupiter on DMP energy $|w|$; dashed lines show dependence $\sigma \propto 1/|w|; 1/w^2$. *Right panel*: Dependence of rescaled captured number of DMP on energy $|w|$ for Jupiter, Saturn and a model planet with $m_p/M_S = 0.004$ (full, dashed, dot-dashed curves respectively).

In a scattering problem at infinity we have $\ell^2 = r_d^2 v_p^2 |w|$ with the impact scattering distance $r_d^2 = 2qr_p/|w|$. Hence, the capture cross section at energy $|w|$ is $\sigma(w)/\sigma_p = (\pi^2 r_p |w|)^{-1} \int_0^{2\pi} d\theta \int_0^{\pi} d\varphi \int_0^{\infty} dq h(q, \theta, \varphi)$, where h is a fraction of DMP captured after one map iteration from $w < 0$ to $w > 0$, given by an interval length inside $F(x)$ envelope at $|w| = const$, $\sigma_p = \pi r_p^2$. This fraction is determined from numerically computed $F(x)$, as those shown in Fig. 1, via a continuous fit spline of function $F(x)$. Using a grid with up to $N_g = 10^5$ points in (q, θ, φ) volume we perform a Monte Carlo integration which gives $\sigma(w)$ as a function of energy w for the case of Jupiter where the main contribution is given by $|w| \sim w_{cap} = m_p/M_S \approx 10^{-3}$. The dependence $\sigma(w)/\sigma_p$ is shown in Fig. 2. For $|w| < w_{cap}$ we find $\sigma/\sigma_p \approx \pi M_S w_{cap}/m_p|w|$ in agreement with analytical estimates [5], for $|w| > w_{cap}$ we have $\sigma/\sigma_p \approx \pi M_S w_{cap}^2/(m_p w^2)$. The later regime describes contribution of close encounters which has a rapid decrease of σ and hence gives a small contribution in the capture process. This conclusion is confirmed by the analysis of the differential number of captured DMP per time unit $dN = \sigma(w) n_g v_p^2 f(w) dw/2$. Here n_g is a galactic DMP density with a corresponding mass density $\rho_g = m_d n_g \sim 4 \cdot 10^{-25} g/cm^3$ [1] and $f(w)$ is the velocity distribution function given above with $v^2 = v_p^2|w|$ at infinity. A number of DMP crossing the planet orbit area per time unit is $N_p = \int_0^1 n_g \sigma_p v_p^2 f(w) dw/2$. The dependence of $dN/N_p dw$ on $|w| = v^2/v_p^2$, presented in Fig. 2, drops quadratically for $|w| > w_{cap}$ showing that the contribution of close encounters is small. We note that $dN/N_p dw$ depends only on the ratio w/w_{cap} that is confirmed by additional data obtained for Saturn and a model planet in Fig. 2. As a result the total number of captured particles is $N \propto m_p M_S$ in agreement with [5].

To determine the number of captured DMP $N_{cap}(t)$, in SS with Jupiter, as a function of time we model numerically a constant flow of scattered particles with energy distribution $dN_s \propto v f(v) dv$ per time unit. The injection, capture, evolution and escape of DMP is described by the dark map (1) with corresponding values of scattered parameters q, θ, φ and corresponding to them $F(x)$ function with the scattering DMP distribution $dN_s \propto dq dw$ (we use $q \leq q_{max} = 4r_p$ since above this value F_{max} is very small). The scattering and evolution processes are followed during the whole life time of SS taken as $t_S = 4.5 \cdot 10^9 years$. The total number of DMP, injected during time t_S in the whole energy range $0 \leq |w| \leq \infty$, is $N_{tot} \approx 1.5 \cdot 10^{14}$ with $N_H = 4 \cdot 10^9$ scattered DMP in the Halley comet range $0 < |w| \leq w_H \approx 0.005$ ($\kappa = N_{tot}/N_H \approx 2u^2/(3v_p^2 w_H) \approx 3.8 \cdot 10^4$, only DMP with $|w| < F_{max}$ participate in dynamics). We used a random grid of initial q, θ, φ values with up to $N_0 = 4 \cdot 10^5$ grid points and N_i injected orbits at each grid point with $N_H = N_0 N_i$.

The time dependence $N_{cap}(t)$ in Fig. 3 shows that initially it grows linearly with time. This growth slows down after a time scale $t_d \approx 10^7$ years. For a finite SS region with $w > 1/20$ we see that there is a saturation of captured number of DMP. Indeed, according to the results for the Halley comet [9] the scale $t_d \sim 10^7 yr$ is a typical

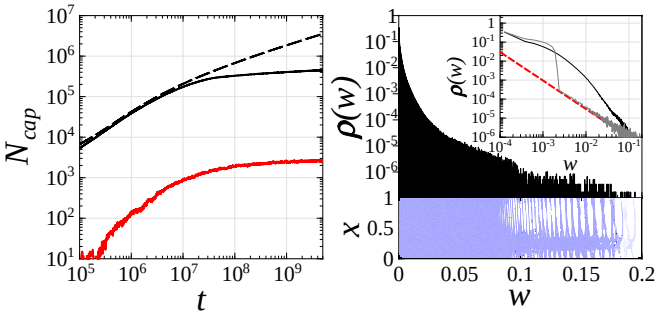

FIG. 3: *Left panel*: The number N_{cap} of captured DMP, as a function of time t in years, for energy range $w > 0$ (dashed curve), $w > 4 \cdot 10^{-5}$ corresponding to half distance between Sun and Alpha Centauri System (black curve), $w > 1/20$ corresponding to $r < 100AU$ (red curve); DMP are injected at constant flow $f(v)$ at all angles. *Right panel*: Top part shows density distribution $\rho(w) \propto dN/dw$ in energy at time t_S for DMP injection at all parameters q, θ, φ (normalized as $\int_0^\infty \rho dw = 1$), bottom part shows the Poincaré section of the dark map for DMP injection at fixed parameters q, θ, φ of Fig. 1b; inset shows density distribution of captured DMP in w in log-log scale for parameters of Fig. 1b (gray curve) and orbits of the main right panel injected at all parameters (black curve), a dashed line shows a slope -3/2.

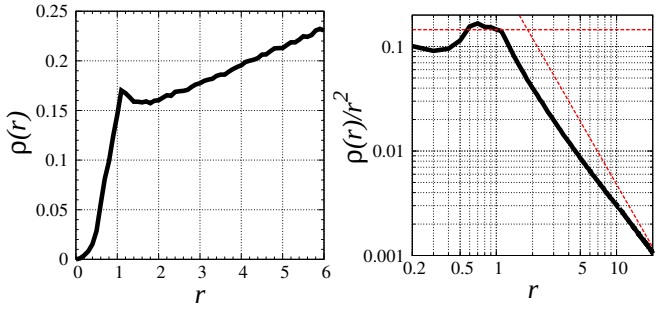

FIG. 4: *Left panel*: Radial density $\rho(r) \propto dN/dr$ at present time t_S for SS with Jupiter averaged over all N_{AC} DMP (the normalization is fixed as $\int_0^{6r_p} \rho dr = 1$, $r_p = r_J = 1$). *Right panel*: Volume density $\rho_v = \rho/r^2$ from the data of left panel, dashed line shows slope -2, horizontal line shows average density for $r_p/5 \le r \le r_p$.

scale of diffusive escape of a comet or DMP from SS due to chaotic diffusion in energy. The analytical estimates given in [5, 9] also give a similar escape time. Thus after that time the injected flow is compensated by the escape process and we obtain a system in an equilibrium state with a fixed number of captured DMP with a certain energy distribution $\rho(w)$. An example of such a distribution for a typical orbit parameters q, θ, φ at present time $t = t_S$ is shown in the inset of the right panel of Fig 3 (gray curve). There is a peak of density at small energies $w < 0.002$ where the orbital period is very long and chaotization is slow. For the range $0.002 < w < w_{ch}$ we have an approximate algebraic decay $\rho \sim 1/w^{3/2}$ which corresponds to the ergodic measure where DMP density is proportional to the orbital period $T_w \sim 1/w^{3/2}$. The chaotic diffusion to large energies is stopped by a critical invariant Kolmogorov-Arnold-Moser (KAM) curve which separates chaos region from integrable one at $w = w_{ch}$. The analytical estimate [5], based on the Chirikov criterion [3, 4], gives for $F_{max} \approx 5m_p/M_S$ the value $w_{ch} \approx 0.3$ that is in a good agreement with the case of Fig. 3 where $w_{ch} \approx 0.2$. In a region $w_{ch}/2 < w < w_{ch}$ we have stability islands, being well visible in the Poincaré section, that gives significant fluctuations in density $\rho(w)$. However, for $w < w_{ch}/2$ the chaos component is homogeneous in the phase plane (w, x). This means that DMP are injected in the chaotic component of a chaotic layer around separatrix $w = 0$, and thus the DMP dynamics in SS is essentially chaotic.

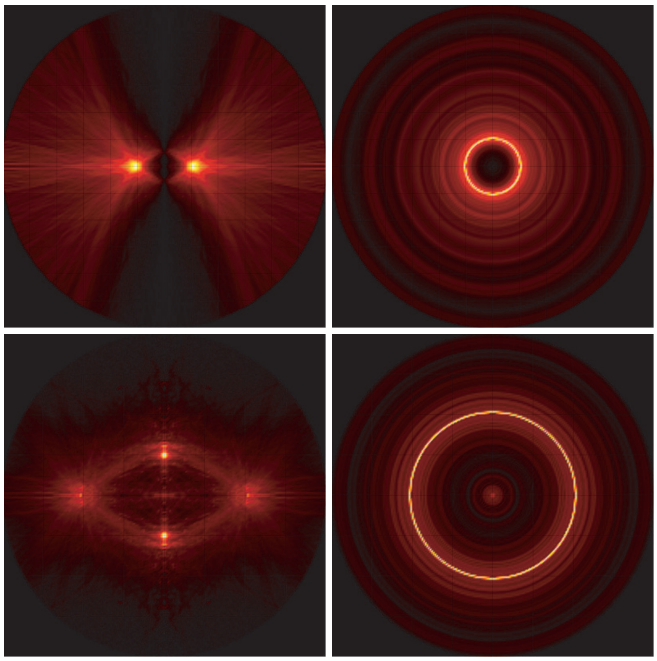

FIG. 5: Density of captured DMP in SS at present time t_S. *Top panels:* DMP surface density $\rho_s \propto dN/dzdr_\rho$ shown at *left* in cross plane $(0, y, z)$ perpendicular to Jupiter orbit (data are averaged over $r_\rho = \sqrt{x^2 + y^2} = const$), at *right* in Jupiter plane $(x, y, 0)$; only the range $|r| \le 6r_J$ around the Sun is shown. *Bottom panels:* corresponding DMP volume density $\rho_v \propto dN/dxdydz$ at *left* in plane $(0, y, z)$, at *right* in Jupiter plane $(x, y, 0)$; only the range $|r| \le 2r_J$ around the Sun is shown. Color is proportional to density with yellow/black for maximum/zero density.

To obtain DMP space density we consider N_{tot} scattered orbits as described above. Their time evolution is described by the dark map (1) up to the present moment of time t_S. We keep in memory the initial orbit parameters q, θ, φ of captured orbits. Then we con-

sider only those with $w > 4 \cdot 10^{-5}$ during the time interval $\delta t_S/t_S = \pm 10^{-3}$ near time moment t_S collecting $\delta N_{AC} \approx 6.2 \cdot 10^6$ orbits (while instantaneously we have $N_{AC} \approx 3.3 \cdot 10^5$). For these δN_{AC} DMP their dynamics in real space is recomputed from their values of q, θ, φ, w, x during the time period of $\Delta t \approx 100$ Jupiter orbital periods using Newton equations. The radial density $\rho(r)$ of DMP is obtained by averaging over 10^3 points randomly and homogeneously distributed over this time interval Δt for each of δN_{AC} orbits. The obtained normalized radial distribution $\rho(r)$ in shown in Fig. 4 with the corresponding average volume density $\rho_v = \rho/r^2$. It corresponds to a stationary equilibrium regime appearing at $t \gg t_d$ when injection and escape flows compensate each other. The striking feature of the obtained result is that for $r > r_p$ we find $\rho(r) \approx const$, This means that the total DMP mass in a radius r grows linearly with r. According to the virial theorem such a profile gives a velocity of visible matter independent of radius $v_m^2 \sim \int_0^r \rho(r')dr'/r \sim \rho(r)$, being similar to those found in galaxies when the DMP mass is dominant [1, 7]. Another important feature is that the DMP volume density ρ_v remains approximately constant for $r < r_p = r_J$. However, for $r > r_J$ this density drops as inverse square distance from the Sun [16]. Thus we find that a simple model of SS with one rotating planet is able to reproduce significant features of observed DMP density distribution in galaxies.

From the data of Figs. 3 we determine the fraction $\eta_{AC} = N_{AC}/N_{tot} \approx 2.2 \cdot 10^{-9}$ of DMP captured at time t_S at energies $w > 4 \cdot 10^{-5}$ and related fraction $\eta_{20} \approx 1.5 \cdot 10^{-11}$ at energies $w > 1/20$. From Fig. 4 we determine the fraction of N_{AC} orbits in the volume $r \leq 6r_p$ with $\eta_{r6} \approx 4.3 \cdot 10^{-4}$ and in the volume $r \leq r_p$ with $\eta_{r1} \approx 2.3 \cdot 10^{-5}$. The DMP mass corresponding to these fractions is obtained by multiplication of these fractions by the total mass of DMP flow passed in the corresponding range $q \leq 4r_p$: $M_{tot} = \int_0^\infty dvvf(v)\sigma\rho_g t_S \approx 69\rho_g t_S k r_p M_S/u \approx 0.9 \cdot 10^{-6} M_S$ where we use the cross section $\sigma = \pi r_d^2 = 8\pi k M_S r_p/v^2$ for injected orbits with $q \leq 4r_p$, k is the gravitational constant ($u/v_p \approx 17$). Thus the mass of DMP with $w > 4 \cdot 10^{-5}$ is $M_{AC} \approx \eta_{AC} M_{tot} \approx 2 \cdot 10^{-15} M_S$, and in a similar way the mass at $w > 1/20$ is $M_{20} \approx \eta_{20} M_{tot} \approx 1.3 \cdot 10^{-17} M_S$. The mass M_{AC} can be estimated as a mass of DPM with $|w| < w_H$ absorbed by $F \sim \sin x$ kick during the diffusion time t_d that gives $M_{AC} \sim v_p^2 w_H t_d M_{tot}/(\pi u^2 t_S) \sim 10^{-8} M_{tot} \sim 10^{-14} M_S$ being only by a factor 5 larger the above numerical value.

The mass of DMP in the volume of Neptune orbit radius $r < 6r_p$ is $M_{r6} = \eta_{r6} M_{AC} \approx 0.9 \cdot 10^{-18} M_S \approx 1.7 \cdot 10^{15} g$ and in the radius $r < r_p$ the DMP mass is $M_{r1} = \eta_{r1} M_{AC} \approx 4.6 \cdot 10^{-20} M_S \approx 10^{14} g$. The average volume density of captured DMP inside the Jupiter orbit sphere $r < r_p = r_J$ is $\rho_J = 3M_{r1}/(4\pi r_p^3) \approx 1.2 \cdot 10^{-4} \rho_g \approx 5 \cdot 10^{-29} g/cm^3$. Thus, the density of captured DMP is much smaller than the galactic DMP density. However, it is by a factor $4 \cdot 10^3$ larger than the equilibrium DMP galactic density $\rho_{gH} \approx 0.25\rho_g/\kappa^{3/2} \approx 1.4 \cdot 10^{-32} g/cm^3$ taken in the energy range $0 < |w| < w_H$.

The density distribution of captured DMP in SS is shown in Fig. 5. We see that the density decreases with r at $r > r_J$ in agreement with Fig. 4. A characteristic bulge is formed around the Jupiter orbit. A maximal local volume density is about 10 times larger than the average density ρ_J inside $r < r_J$.

For further studies it is desirable to take into account the contribution of other planets even if the results presented in [9] show that the main features of the dynamics are well described only by Jupiter contribution considered here. It is natural to expect that, as in the SS with one planet, the DMP dynamics in galaxies is dominated by a few stars rotating around the central black hole and thus an approximately constant radial DMP density found here behind Jupiter orbit should be typical for such galaxies in agreement with observational data [7].

We thank I.B.Khriplovich for useful discussions. A part of numerical computations has been performed at the mésocentre de calcul de Franche-Comté.

[1] G. Bertone,D. Hooper and J. Silk, *Particle dark matter: evidence, candidates and constraints*, Phys. Rep. **405**, 279 (2005).

[2] M. Valtonen and H. Karttunen, *The Three-Body Problem*, Cambridge Univ. Press, Cambridge, UK, (2005).

[3] B.V.Chirikov, *A universal instability of many-dimensional oscillator systems*, Phys. Rep. **52**, 263 (1979).

[4] A.J.Lichtenberg and M.A.Lieberman, *Regular and chaotic dynamics*, Springer, Berlin (1992).

[5] I.B.Khriplovich and D.L.Shepelyansky, *Capture of dark matter by the Solar System*, Int. J. Mod. Phys. D **18**, 1903 (2009).

[6] A.H.G. Peter, *Dark matter in the Solar System. I. The distribution function of WIMPs at the Earth from solar capture*, Phys. Rev. D **79**, 103531 (2009); *Dark matter in the Solar System. III. The distribution function of WIMPs at the Earth from solar capture*, **ibid. 79**, 103533 (2009).

[7] V.C. Rubin, W. K. Ford, Jr. and N. Thonnard, *Rotational properties of 21 Sc galaxies with a large range of luminosities and radii from NGC 4605 (R=4kpc) to UGC 2885 (R=122kpc)*, Astrophys. Jour. **238**, 471 (1980).

[8] T.Y. Petrosky, *Chaos and cometary clouds in the Solar System*, Phys. Lett. A **117**, 328 (1986).

[9] B.V. Chirikov and V.V. Vecheslavov, *Chaotic dynamics of comet Halley*, Astron. Astrophys. **221**, 146 (1989).

[10] M. Duncan, T. Quinn and S.Tremaine, *The long-term evolution of orbits in the Solar System: a mapping approach*, Icarus **82**, 402 (1989).

[11] R. Dvorak and J. Kribbel, *Dynamics of Halley-like comets for 1 million years*, Astron. Astrophys. **227**, 264 (1990).

[12] L. Malyshkin and S.Tremaine, *The Keplerian map for the*

planar restricted three-body problem as a model of comet evolution, Icarus **141**, 341 (1999).

[13] D.L.Shepelyansky, *Microwave ionization of hydgoren atoms*, Scholarpedia **7(1)**, 9795 (2012).

[14] A. Gould and S.M.K. Alam, *Can heavy WIMPs be captured by the Earth?*, Astrophys. J. **549**, 72 (2001).

[15] J. Lundberg and J. Edsjö, *Weakly interacting massive particle diffusion in the solar system including solar depletion and its effect on Earth capture rates*, Phys. Rev. D **69**, 123505 (2004).

[16] A formal fit of data of Fig. 4 right panel in the range $2 < r/r_p < 20$ gives $\rho_v \sim 1/r^\beta$ with $\beta = 1.53 \pm 0.002$. We can argue that this dependence can be understood from the ergodic measure of effectively one-dimentional chaotic radial dynamics: $d\mu \sim dN \sim \rho dr \sim \int dt dw dN/dw \sim dt \sim dr/v_r \sim \sqrt{r} dr$ (assuming that dN/dw is peaked near $w \approx 0$ as it is seen in the inset of Fig.3 and hence the radial velocity $v_r \sim \sqrt{1/r - w} \sim 1/\sqrt{r}$ and $\rho_v \sim 1/r^{3/2}$). However, we perform the density analysis mainly inside the Neptune orbit where the radial density $\rho(r)$ can be considered as approximately constant.